

Assessment of pushover-based method to a building with bidirectional setback

Kenji Fujii*

Department of Architecture, Chiba Institute of Technology, 2-17-1 Tsudanuma, Narashino, Chiba 275-0016, Japan

(Received March 3, 2016, Revised August 16, 2016, Accepted September 3, 2016)

Abstract. When conducting seismic assessment of an asymmetric building, it is essential to carry out three-dimensional analysis considering all the possible directions of seismic input. For this purpose, the author proposed a simplified procedure is to predict the largest peak seismic response of an asymmetric building subjected to horizontal bidirectional ground motion acting in an arbitrary angle of incidence in previous study. This simplified procedure has been applied to torsionally stiff (TS) asymmetric buildings with regular elevation. However, the suitability of this procedure to estimate the peak response of an asymmetric building with vertical irregularity, such as an asymmetric building with setback, has not been assessed. In this article, the pushover-based simplified procedure is applied to estimate the peak response of asymmetric buildings with bidirectional setback. Nonlinear dynamic (time-history) analysis of two six-storey asymmetric buildings with bidirectional setback and designed according to strong-column weak beam concept is carried out considering various directions of seismic input, and the results compared with those estimated by the proposed method. The largest peak displacement estimated by the simplified method agrees well with the envelope of the dynamic analysis response. The suitability assessment of the simplified procedure to analysed building models is made as well based on pushover analysis results.

Keywords: asymmetric building; setback; pushover analysis; bidirectional excitation; torsional index; angle of incidence of seismic input

1. Introduction

Estimating the peak response of buildings that may be subjected to strong ground motion is important for good seismic design of new buildings and seismic assessment of existing buildings (ATC-40 1996, FEMA 1997, CEN 2004, and ASCE 2007). To analyse a building's response, the building model is subjected to horizontal ground motion acting on each of the main orthogonal axes of the building. However, for seismic assessment of asymmetric buildings this procedure may be inadequate because the most critical direction of incidence of the seismic input, which would produce the largest response, may be different from the direction of the building's main orthogonal axes, and the major component of the ground motion may act in any direction. Therefore, it is essential to carry out three-dimensional analyses considering all the possible directions of seismic

*Corresponding author, Professor, E-mail: kenji.fujii@it-chiba.ac.jp

input. It is widely accepted that the most rigorous method to evaluate the seismic response of a building is the nonlinear dynamic (time-history) analysis of a multi-degree-of-freedom (MDOF) model. However, it is very time-consuming to evaluate the response of a building under all possible seismic intensities and all possible directions of incidence of seismic input. Therefore, it may not be suitable for common structural design work carried out in most design offices.

Simplified nonlinear analysis procedures combine the nonlinear static (pushover) analysis of a MDOF model and the response spectrum analysis of an equivalent single-degree-of-freedom (SDOF) model (Saiidi and Sozen 1981, Fajfar and Fischinger 1988). These procedures have been widely implemented in seismic design codes and seismic evaluation schemes (ATC-40 1996, FEMA 1997, CEN 2004, ASCE 2007), and they work well for buildings that oscillate predominantly with a single mode. In recent decades, several researchers have tried to extend these simplified procedures to improve the seismic performance estimates of buildings with plan and/or elevation irregularities, such as Moghadam and Tso (1996, 2000), Chopra and Goel (2004), Fajfar *et al.* (2005), D'Ambrisi *et al.* (2009), Kristin and Fajfar (2010, 2012), Reyes and Chopra (2011a, b), Bhatt and Bento (2011, 2012, 2014), Bosco *et al.* (2012, 2013, 2015), Manoukas *et al.* (2012, 2014), Cimellaro *et al.* (2014), and Fujii (2011, 2014, 2015, 2016). Recent investigations of the extension of this simplified procedure to an irregular structure can be found in Lavan and De Stefano (2013) and in Zembaty and De Stefano (2016). Reviews of the research on the seismic behaviour of irregular building structures over the last decade can be found in De Stefano and Pintucchi (2008), and Anagnostopoulos *et al.* (2015). Most of these studies focused on the extension of the simplified procedure to asymmetric buildings with regular elevation, while a few of them studied asymmetric buildings with setbacks (Moghadam and Tso 2000, D'Ambrisi *et al.* 2009, and Cimellaro *et al.* 2014). However, the majority of the buildings in city centres have both plan irregularities and vertical irregularities (such as setback); therefore, validation and extension of this simplified procedure for buildings with plan and vertical irregularities are needed.

From the author's point of view, there are four possible approaches when considering the torsional effect for predicting the peak response of asymmetric buildings. The first approach is a combination of nonlinear pushover analysis and linear dynamic analysis (Peruš and Fajfar 2005, Fajfar *et al.* 2005). The second approach is a combination of nonlinear pushover analysis representing several modal responses with the application of the square-root-of-sum-of-squares (SRSS) or complete quadratic combination (CQC) rules, as proposed by Chopra and Goel (2002, 2004). The third approach combines two pushover analyses and envelopes the results, as proposed by Bosco *et al.* (2012, 2013, 2015). The fourth approach is a combination of the analyses of two independent equivalent SDOF models representing the first and second modes and the envelope of four pushover analyses that includes the effect of bidirectional excitation (Fujii 2011, 2014), assuming that the first and second modes are predominantly (or purely) translational modes.

The first approach, named the *Extended N2 method*, is the extended version of the simplified procedure proposed by Fajfar and Fischinger (1988). In this procedure, the peak response of each frame is estimated using the pushover analysis results multiplied by a "correction factor", which is defined using linear dynamic analysis and pushover analysis results (Peruš and Fajfar 2005, Fajfar *et al.* 2005). This approach was verified by Bhatt and Bento (2011). In recent years, the extended N2 method was modified by Kristin and Fajfar (2010, 2012) by considering the elastic response displacement in both plan and elevation. The modification is expressed as the product of c_E and c_T , where c_E is the correction factor in the vertical, and c_T is the correction factor in the horizontal plane (torsional effect). They assumed that c_E does not depend on the position in the horizontal plane while c_T is independent of the floor level and is determined based on the displacement at the

roof (top floor). Bhatt and Bento proposed an extended version of the adaptive capacity spectrum method (Bhatt and Bento 2012, 2014). In their studies, the higher-mode effect on the vertical distribution of the response displacement is considered by using the displacement-based adaptive pushover (DAP) analysis method proposed by Antoniou and Pinho (2004), while the torsional effect is considered by applying Fajfar's approach. The applicability of the extended N2 method to an asymmetric building with setback is examined by D'Ambrisi *et al.* (2009), while Cimellaro *et al.* (2014) proposed a bidirectional pushover analysis (BPA), which is the modified version of the extended N2 method that considers simultaneous loading within the pushover analysis, and is applied to asymmetric buildings with setback.

The extended N2 method is based on the assumption that the elastic envelope of lateral displacement is conservative with respect to the inelastic envelope, as noted by De Stefano and Pintucchi (2010). They pointed out that this assumption may be invalid for structures characterized by very high torsional stiffness. Isakovic and Fischinger (2011) performed shaking table tests on a reinforced concrete (RC) bridge structure and showed that the extended N2 method failed to estimate the peak responses under high seismic intensity because it did not take into account changes in the fundamental mode. In the latest version of the extended N2 method proposed by Kristin and Fajfar (2010, 2012), their assumptions that c_T is independent of the floor level may be valid if the centres of mass (CMs) of all the floors lie along the same vertical axis. However, their approach may be invalid in case of an asymmetric building with setback where the CMs do not lie along the same vertical axis. Additionally, in such a building the definition of c_T for the frames which do not reach the top floor is questionable, since c_T is determined based on the displacement at the top floor.

The second approach, called *modal pushover analysis* (MPA), was proposed by Chopra and Goel (2002) for regular buildings considering the higher-mode effect, and was extended for asymmetric buildings (Chopra and Goel 2004). The MPA was further extended by Reyes and Chopra (2011a, 2011b) who took into account the effect of bidirectional excitation. In this approach, the seismic response is estimated using pushover analysis of a MDOF model with an invariant force distribution based on each elastic mode shape, estimation of the peak response of the independent equivalent SDOF models, and the combination rules that are usually applied in linear analysis (the SRSS or CQC rule). Manoukas *et al.* (2012) and Manoukas and Avramidis (2014) proposed a procedure similar to MPA. The main difference between their procedure and MPA is that they considered the effect of bidirectional excitation in the formulation of the equivalent SDOF model, while in MPA by Reyes and Chopra (2011a, 2011b) the combination of the bidirectional excitation is considered by the SRSS rule.

From the author's point of view, using the second approach to analyse asymmetric buildings with setback presents fewer obstacles than using the first approach. However, the applicability of the second approach depends strongly on whether the change in the mode shape in the inelastic range is significant. As shown by the author in a previous study (Fujii 2015), the estimated results based on the elastic mode shape may provide erroneous results when the change in the mode shape is significant. To overcome the shortcoming of MPA, Belejo and Bento (2016) has applied an improved modal pushover analysis (IMPA), which is the modified version of MPA by considering the change in the mode shape in the inelastic range, to three-storey building (SPEAR building) and nine storey building. It is interesting to note that the mode shape in the inelastic range is approximated based on conventional (non-adaptive) force-based pushover analysis carried out several times in their IMPA, which may be easy to apply for common design work.

The third approach, which was proposed by Bosco *et al.* (2012), estimates the peak response at

the stiff and flexible-side frames by enveloping two pushover analyses results. Bosco *et al.* (2015) investigated the applicability of this procedure to multi-storey building models with the same geometry in each floor. In this procedure, “corrective eccentricity” is the key parameter in the pushover analyses. This may be a promising approach because the various possible collapse mechanisms resulting from the combination of several modal responses can be properly predicted using a combination of different force distributions. However, it may be very difficult to apply this directly to buildings with setback. One of the problems is that three parameters - the stiffness, strength eccentricities and uncoupled frequency ratio - are needed to calculate the corrective eccentricity for each storey; the stiffness eccentricity and uncoupled frequency ratio of each storey may be determined as shown in their studies (Bosco *et al.* 2013). However, estimating the strength eccentricity of each storey is difficult because it may depend strongly on the distribution of the lateral forces. Another problem arises, as in the first approach, when the CMs of all the floors in a building with setback do not lie along the same vertical axis, making it difficult to determine the proper corrective eccentricity.

The fourth approach has fewer obstacles than the other approaches when applied to asymmetric buildings with setback. In the first version of the procedure (Fujii 2011), the applicability was limited to asymmetric buildings with regular elevation and the same geometry in each floor, because the conversion step from the multi-storey building model to an equivalent single-storey model was needed. The latest version of this method (Fujii 2014) overcomes this limitation by developing the displacement-based mode-adaptive pushover (DB-MAP) analysis for a multi-storey frame structure, which can account for changes in the mode shape at each nonlinear stage; in the latest version, the multi-storey building model can be directly converted to equivalent SDOF models. Therefore, theoretically, this procedure should be applicable *without any modification*, to an asymmetric building with setback as long as the building satisfies the following conditions: (a) the building oscillates predominantly in a single mode in each set of orthogonal directions, (b) the principal directions of the first and second modal responses are almost orthogonal. Thus, this approach has the potential to improve the estimate of the response of asymmetric buildings with setback. It should be noted that the main differences from MPA procedure proposed by Chopra *et al.* are a) the change of mode shape beyond elastic range is considered (mode-adaptive), b) the formulation of equivalent SDOF model is based on the principal direction of the each modal response, c) the effects of simultaneous bi-directional excitation is considered by using the combinations of four pushover analyses, not SRSS rule.

In this article, the ability of the pushover-based procedure proposed by the author (Fujii 2014), to estimate the peak response of asymmetric buildings with bidirectional setback is assessed. In the numerical examples, nonlinear time history analysis of two six-storey asymmetric buildings with bidirectional setback and designed according to strong-column weak beam concept is carried out and the building’s response to seismic input from various directions is compared with the results of the simplified method.

2. Outline of the simplified procedure

An outline of the simplified procedure for estimating the “largest” peak response is summarized in Fig. 1. The asymmetric building considered in this study is an N -storey building, with $3N$ degrees of freedom ($3N$ -DOFs). All the frames of the asymmetric building are oriented in the X or Y directions, which are orthogonal. Another set of orthogonal axes U and V in the X-Y

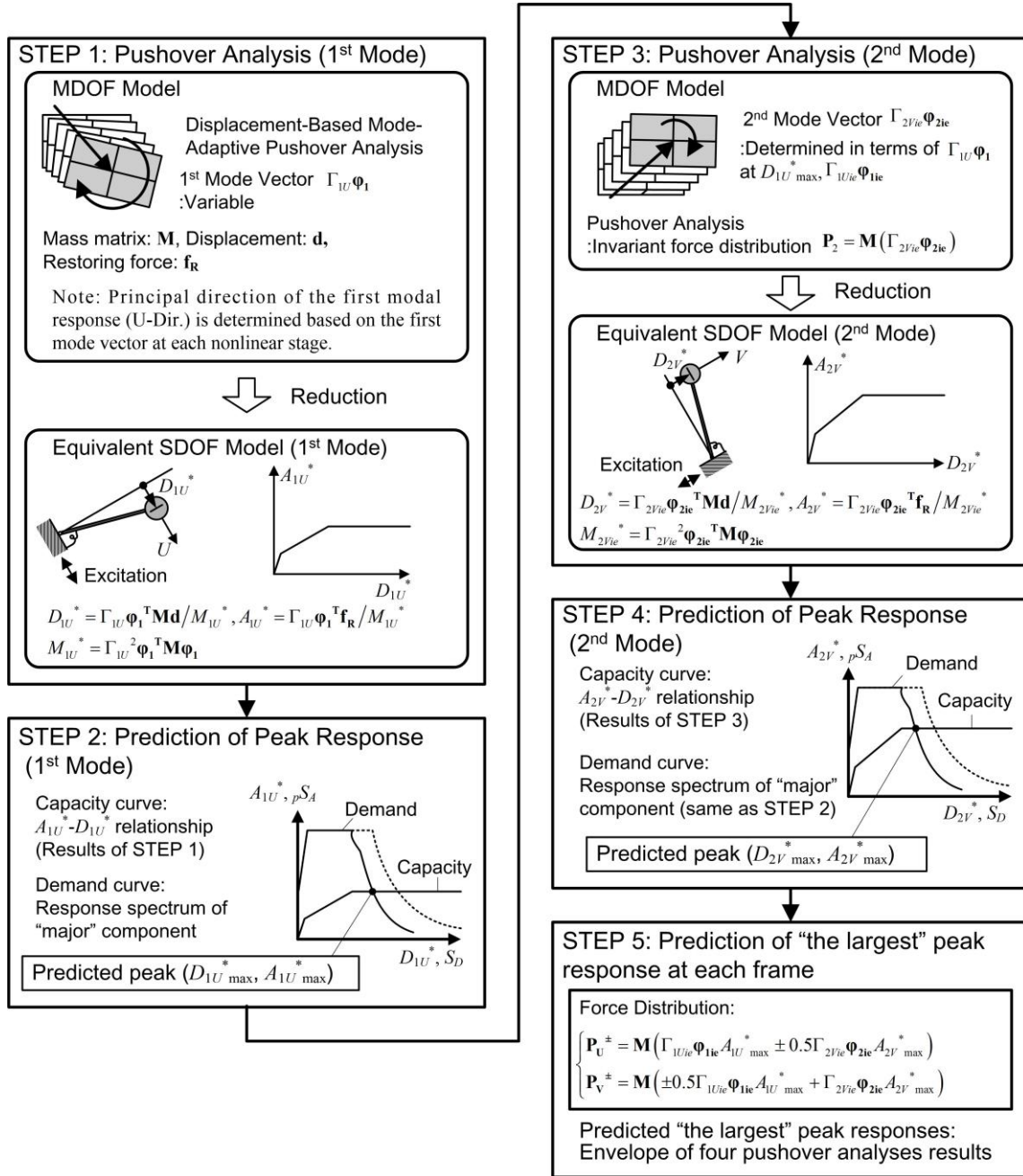


Fig. 1 Outline of the simplified procedure for estimating the peak response of an asymmetrical building (Fujii 2014)

plane is considered, with the U-axis being the principal axis of the first modal response (Fujii 2011, 2014). The fundamental assumptions of the proposed procedure are as follows:

- 1) The spectra of the two horizontal ground-motion components are assumed to be identical to

the response spectrum of the major components.

- 2) The building oscillates predominantly in a single mode in each set of orthogonal directions.
 - 3) The principal directions of the first and second modal responses are almost orthogonal.
- Details of the procedure can be found in Fujii (2014, 2015).

3. Buildings and ground motion data

3.1 Building data

3.1.1 Description of model buildings

In this study, two RC six-storey asymmetric buildings were investigated. Figs. 2 and 3 show the plans of each floor level and the elevations and overview of Models 1 and 2.

The height of the first storey is 4.0 m and the upper storeys are 3.2 m high. The floor mass m_j and moment of inertia I_j ($j=1-6$) are determined assuming a unit mass of 1.2 t/m². The cross sections of the beams are 400×1100 mm at level Z0 (foundation level), and at levels Z1 to Z6 they are 400×700 mm. The cross sections of all the columns are 600×600 mm. The compression strength of the concrete, σ_B , is assumed to be 24 N/mm². In addition, SD 345 steel (yield strength: $\sigma_y=345$ N/mm²) is used for the longitudinal reinforcement while SD 295 steel ($\sigma_y=295$ N/mm²) is used for the shear reinforcement. Each frame structure is designed according to the strong-column

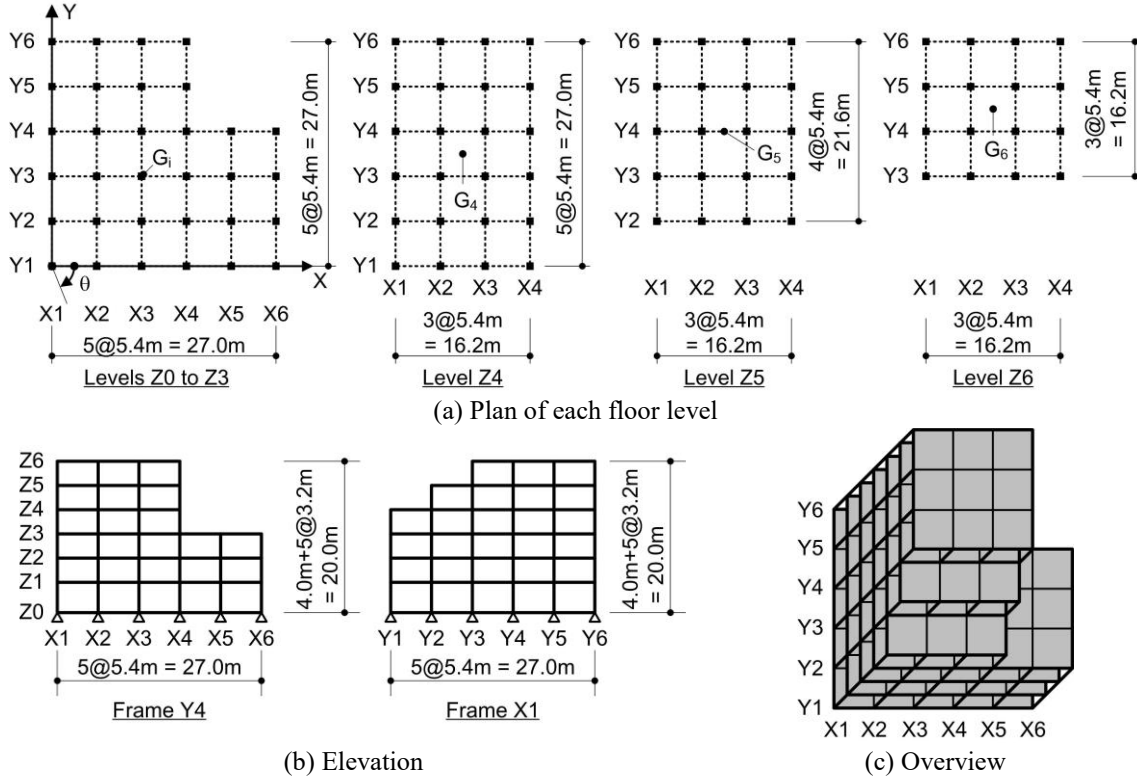


Fig. 2 Model of the building used in the comparative analysis (Model 1)

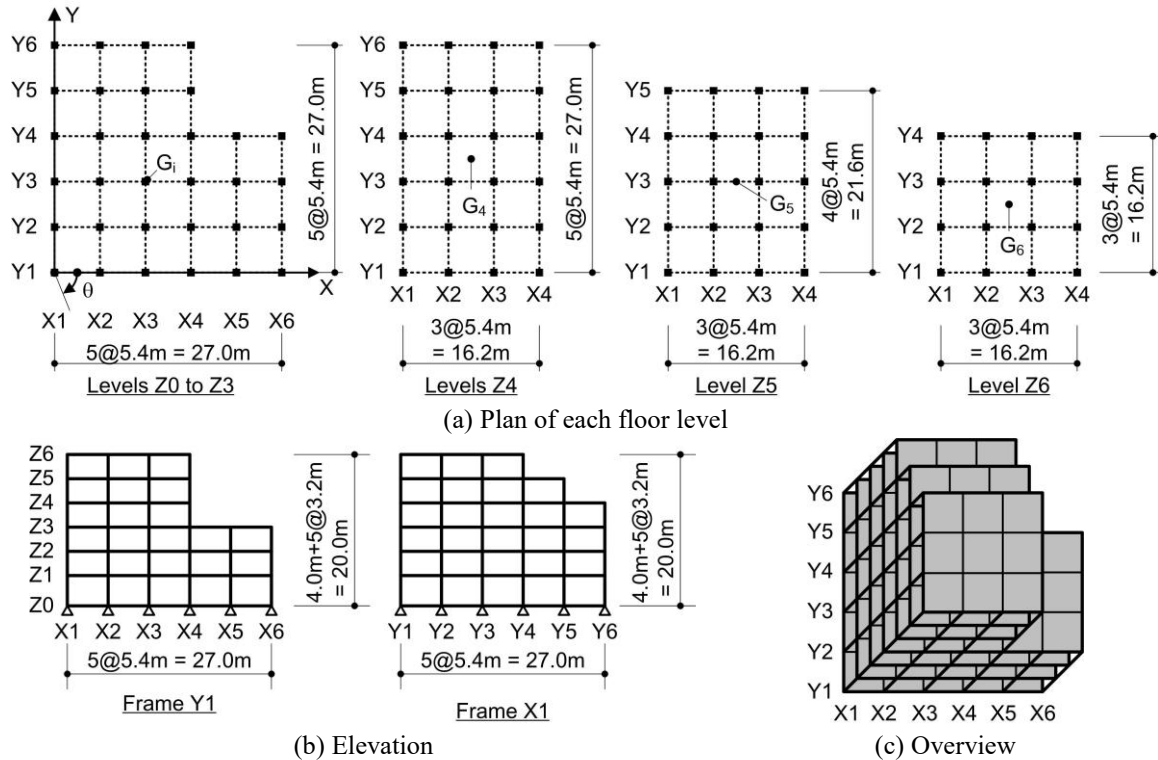


Fig. 3 Model of the building used in the comparative analysis (Model 2)

weak-beam concept; the longitudinal reinforcements of the concrete sections are determined so that potential hinges are located at all the beam ends (except at the foundation level) and at the foot of the columns in the first storey.

The list of longitudinal reinforcement of members are shown in Appendix. The model assumes that sufficient shear reinforcement is provided to prevent premature shear failure.

3.1.2 Mathematical modelling

The building structures are modelled as a pseudo three-dimensional frame model, in which the floor diaphragms are assumed to be rigid in their own planes with no out-of-plane stiffness, and the frames oriented in the X and Y directions are modelled independently. A one-component model, with one nonlinear flexural spring at each end and one shear spring in the middle of the line element is used for all the beams and columns. At the end of each member, rigid zones are assumed, and the rigid zone length is assumed to be half the depth of the intersecting member minus one-fourth of the depth of the considered member. To determine the flexibility of the nonlinear flexural springs, an anti-symmetric curvature distribution is assumed for all the beams and columns.

Fig. 4 shows the moment-rotation relationship of each nonlinear flexural spring. The envelopes of the flexural springs of each member are assumed to be symmetric in both the positive and negative loading directions. In Fig. 4(a), the crack moment M_c , yield moment M_y , and the secant stiffness degradation ratio at the yield point α_y are calculated according to the AIJ Design

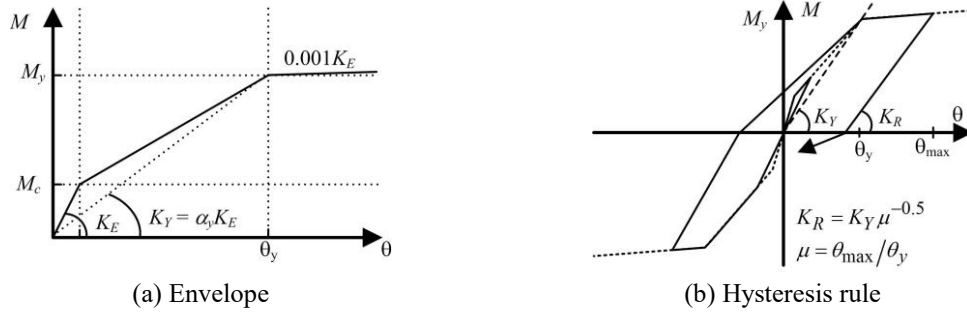


Fig. 4 Moment-rotation relationship of nonlinear flexural spring

Guideline (AIJ 1999); note that the range of α_y is 0.178-0.307 for the beams and 0.275-0.402 for all the columns. The shear behaviour of all the members and the axial behaviour of the columns are assumed to remain elastic, and the effects of biaxial bending and axial-flexural interaction are ignored. The torsional stiffness of the members is also ignored. No second-order effect (e.g., the P- Δ effect) is considered. For the hysteresis model of the nonlinear flexural spring, the Muto hysteresis model (Muto *et al.* 1974) with one modification (Fig. 4(b)) is used. Specifically, the unloading stiffness after yielding decreases in proportion to $\mu^{-0.5}$ (where μ is the ductility ratio of the flexural spring) to represent the degradation of the unloading stiffness after yielding of the RC members. Note that in the formulation of the DB-MAP analysis presented in Fujii (2014), the perfectly symmetric behaviour of all nonlinear springs in structural model is assumed. To satisfy this assumption, the moment-rotation relationship of all nonlinear flexural springs are assumed perfectly symmetric and the average value of M_c , M_y , and α_y in positive and negative loading are used in this study.

The base shear coefficients obtained from the planar pushover analysis in the X and Y directions, which are the values when the displacement at level Z6 (top floor) reaches 1% of the total height H_N (=20.0 m), were 0.347 and 0.348, respectively, for both Models 1 and 2. The damping matrix is assumed to be proportional to the instant stiffness matrix with 3% of the critical damping for the first mode.

3.1.3 Natural modes of the building models

Figs. 5 and 6 show the natural modes of the building models in the elastic range. Here, T_{ie} (i : the natural mode number) is the i th natural period in the elastic range, ψ_{ie} is the angle of incidence of the principal direction of the i th modal response in the elastic range (with its tangent given by Eq. (1)), m_{ie}^* is the i th effective (equivalent) modal mass ratio with respect to the principal direction of the i th modal responses given by Eq. (2), and $R_{\rho ie}$ is the torsional index of the i th mode (Fujii 2014) in the elastic range defined by Eq. (3)

$$\tan \psi_{ie} = - \frac{\sum_j m_j \phi_{Yjie}}{\sum_j m_j \phi_{Xjie}}, \quad (1)$$

$$m_{ie}^* = \frac{1}{\sum_j m_j} \cdot \frac{\left(\sum_j m_j \phi_{Xjie} \right)^2 + \left(\sum_j m_j \phi_{Yjie} \right)^2}{\sum_j m_j \phi_{Xjie}^2 + \sum_j m_j \phi_{Yjie}^2 + \sum_j I_j \phi_{\Theta jie}^2}, \quad (2)$$

$$R_{pie} = \sqrt{\sum_j I_j \phi_{\Theta jie}^2 / \left(\sum_j m_j \phi_{Xjje}^2 + \sum_j m_j \phi_{Yjje}^2 \right)}. \tag{3}$$

In Eqs. (1)-(3), $\Phi_{ie} = \{\phi_{X1ie} \cdots \phi_{XNie} \quad \phi_{Y1ie} \cdots \phi_{YNie} \quad \phi_{\Theta 1ie} \cdots \phi_{\Theta Nie}\}^T$ is the i th natural mode vector in the elastic range. The principal direction of the i th modal response is the direction which maximize the i th effective modal mass ratio, and corresponds to the direction of base shear of the i th mode. The ratio m_{ie}^* is that to evaluate the contribution of the i th modal response to the whole response when the unidirectional excitation acts in the principal direction of the i th modal response, and m_{ie}^* must have a value from 0 to 1; if m_{ie}^* is close to one, the i th modal response is predominant, while if m_{ie}^* is close to zero, the contribution of the i th modal response is very small. The torsional index R_{pie} is zero when the i th mode is purely translational ($\sum_j I_j \phi_{\Theta jje}^2 = 0$).

The relation between m_{ie}^* and R_{pie} is clear when Eq. (2) is rewritten in form of Eq. (4)

$$m_{ie}^* = \frac{1}{\sum_j m_j} \cdot \frac{\left(\sum_j m_j \phi_{Xjje} \right)^2 + \left(\sum_j m_j \phi_{Yjje} \right)^2}{\sum_j m_j \phi_{Xjje}^2 + \sum_j m_j \phi_{Yjje}^2} \cdot \frac{1}{1 + R_{pie}^2}. \tag{4}$$

From this equation it is seen that the ratio m_{ie}^* is close to zero when the torsional index R_{pie} is significantly large. Therefore, as discussed in previous studies (Fujii 2014, 2016), the terms “predominantly translational” and “predominantly torsional” are defined using the index R_{pie} ; the “predominantly translational” mode is the mode when $R_{pie} < 1$, while the “predominantly torsional” mode is the mode when $R_{pie} > 1$. Note that the definition of ψ_{ie} , m_{ie}^* and R_{pie} shown in Eqs. (1)-(3) is extended in case the building oscillates beyond the elastic range later in section 5, by replacing the the i th natural mode vector in the elastic range to that in each nonlinear stage.

As shown in Figs. 5 and 6, the principal directions of the first three modes are not along the X and Y axes in any of the building models. In both building models, the first mode is predominantly translational ($R_{p1e} < 1$), the second mode is almost purely translational ($R_{p2e} \ll 1$), while the third mode is predominantly torsional ($R_{p3e} > 1$); the angles between the principal directions of the first two modes is close to 90° (90.5° for Model 1, and 90.0° for Model 2).

It should be also pointed out that from Figs. 5 and 6, when these buildings oscillate in the first mode, the larger displacement is expected at frames Y6 and X1 in Model 1, while in Model 2 the larger displacement is expected at frames Y1 and X1. Therefore, in Model 1 frames Y6 and X1

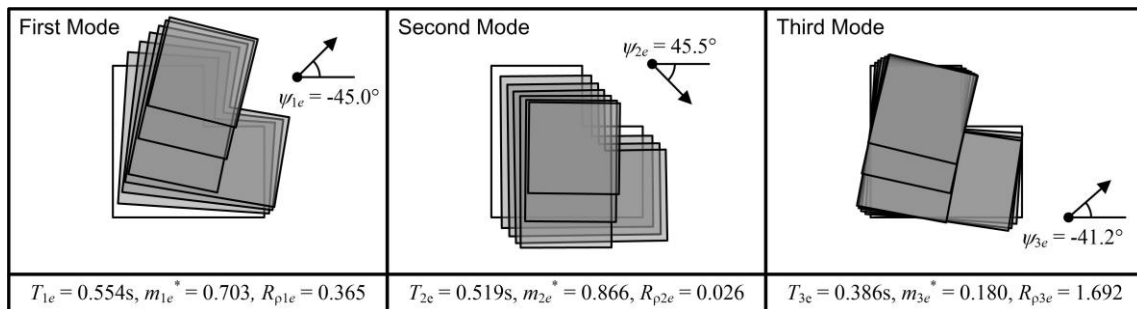


Fig. 5 Shapes of the first three modes of the building models in the elastic range (Model 1)

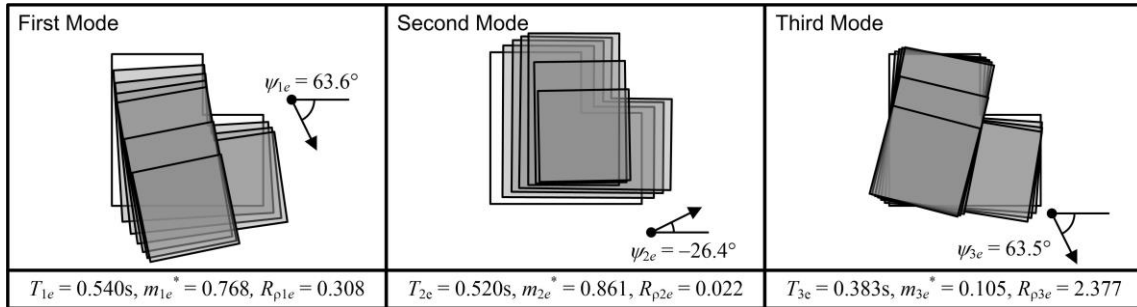


Fig. 6 Shapes of the first three modes of the building models in the elastic range (Model 2)

may be considered as “flexible-edge” frames, while frames Y1 and X6 may be considered as “stiff-edge” frames. Similarly in Model 2, frames Y1 and X1 may be considered as “flexible-edge” frames, while frames Y6 and X6 may be considered as “stiff-edge” frames.

3.2 Ground motion data

In this study, the seismic excitation was considered to be bidirectional in the X-Y plane, and three sets of artificial ground motions (referred to as Art-001, 002 and 003) were generated.

The target elastic response spectrum of the “major” components with 5% critical damping, ${}_pS_{A\zeta}(T, 0.05)$, determined from the Building Standard Law of Japan (BCJ, 2010) which takes into account the soil condition, was calculated using Eq. (5) as a function of T , the natural period of the SDOF model

$${}_pS_{A\zeta}(T, 0.05) = \begin{cases} 4.8 + 48T \text{ m/s}^2 & : T \leq 0.16s \\ 12.0 & : 0.16s \leq T \leq 0.576s \\ 12.0(0.576/T) & : T \geq 0.576s \end{cases} \quad (5)$$

The target elastic response spectrum of the “minor” components, ${}_pS_{A\zeta}(T, 0.05)$ is reduced by the parameter γ . According to López *et al.* (2006), the ratio of the two responses varies between 0.63 and 0.81, with an average ratio of 0.70. Therefore, the parameter γ was set to 0.7 in this study.

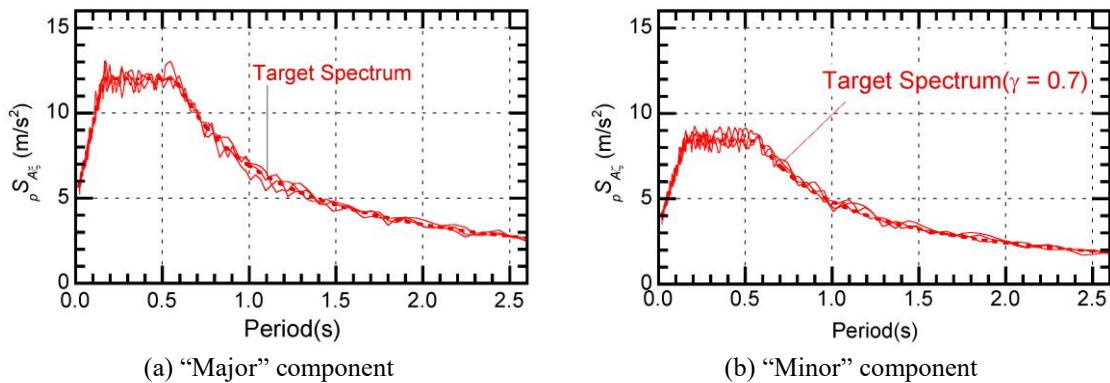


Fig. 7 Elastic pseudo acceleration response spectra for simulated ground motions

The phase angle is given by uniform random values, and to consider the time-dependent amplitude of ground motions, the Jennings type envelope function $e(t)$ proposed by the Building Centre of Japan

$$e(t) = \begin{cases} (t/5)^2 & : 0s \leq t \leq 5s \\ 1 & : 5s \leq t \leq 35s \\ \exp\{-0.027(t-35)\} & : 35s \leq t \leq 120s \end{cases} \quad (6)$$

Fig. 7 shows the elastic response spectra for the major and minor acceleration components of the artificial ground motion with 5% critical damping.

4. Analysis results

4.1 Estimation of the largest peak response using the simplified procedure

Estimates of the largest peak response of the first and second mode responses derived by the equivalent linearization technique (steps 2 and 4) are shown in Figs. 8(a) and (b). The intersection points of the capacity curve and demand curve represent the predicted peak response. The estimated peak equivalent displacement and acceleration of the first mode, D_{1U}^* and A_{1U}^* and those of the second mode, D_{2V}^* and A_{2V}^* , respectively, are shown in these figures.

To estimate the peak responses at each frame, the force distributions used in the pushover analyses (step 5) should be determined. Fig. 9 shows the first- and second-mode vectors corresponding to the estimated peak equivalent displacement of the first mode D_{1U}^* , $\Gamma_{1Uie}\Phi_{1ie}$ and $\Gamma_{2Vie}\Phi_{2ie}$. The combined force distributions used for the pushover analyses can then be determined according to Eq. (7)

$$\begin{cases} \mathbf{P}_U^\pm = \mathbf{M}(\Gamma_{1Uie}\Phi_{1ie}A_{1U}^* \pm 0.5\Gamma_{2Vie}\Phi_{2ie}A_{2V}^*) \\ \mathbf{P}_V^\pm = \mathbf{M}(\pm 0.5\Gamma_{1Uie}\Phi_{1ie}A_{1U}^* + \Gamma_{2Vie}\Phi_{2ie}A_{2V}^*) \end{cases} \quad (7)$$

$$\mathbf{M} = \begin{bmatrix} \mathbf{M}_0 & \mathbf{0} & \mathbf{0} \\ \mathbf{0} & \mathbf{M}_0 & \mathbf{0} \\ \mathbf{0} & \mathbf{0} & \mathbf{I}_0 \end{bmatrix}, \mathbf{M}_0 = \begin{bmatrix} m_1 & & 0 \\ & \ddots & \\ 0 & & m_N \end{bmatrix}, \mathbf{I}_0 = \begin{bmatrix} I_1 & & 0 \\ & \ddots & \\ 0 & & I_N \end{bmatrix}, \quad (8)$$

where \mathbf{M} is the mass matrix of the building model. The combined force distribution used in step 5 is shown in Fig. 10. Note that in this figure the vertical distributions of the horizontal forces and moments are not invert-triangular shape, unlike the mode shape shown in Fig. 9. This is because the mass and moment of inertia of the floor differs significantly at each floor.

The distribution of the estimated relative peak horizontal displacement at each frame in the X and Y directions is shown in Fig. 11. The envelope of the four pushover analyses results is the predicted peak response at each frame. In Fig. 11(a), the predicted peak responses were determined from the results of the pushover analyses using \mathbf{P}_V^+ and \mathbf{P}_V^- for most of the frames in the case of Model 1, while for Model 2 (Fig. 11(b)), the predicted peak responses were determined from all four pushover analyses results.

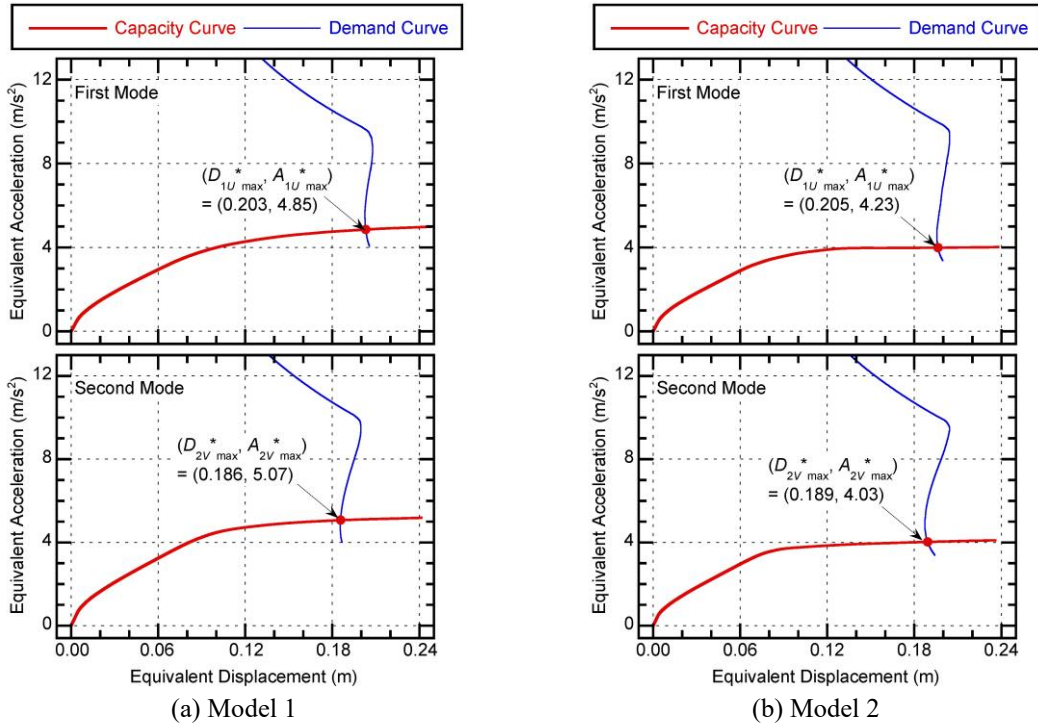


Fig. 8 Estimates of the peak responses of the first and second modes calculated by the equivalent linearization technique

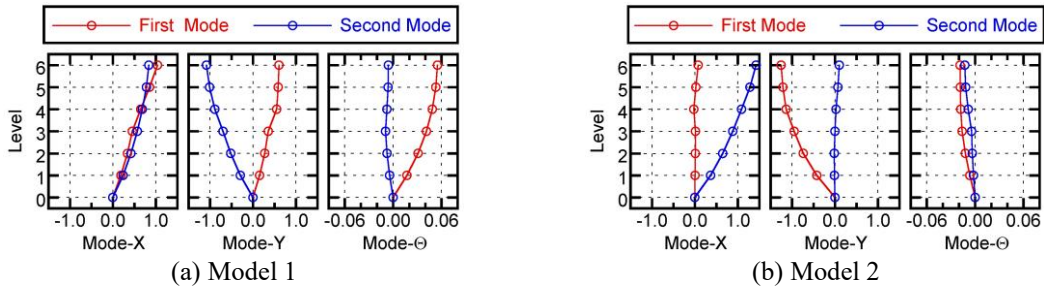


Fig. 9 First- and second-mode vectors corresponding to the predicted peak response

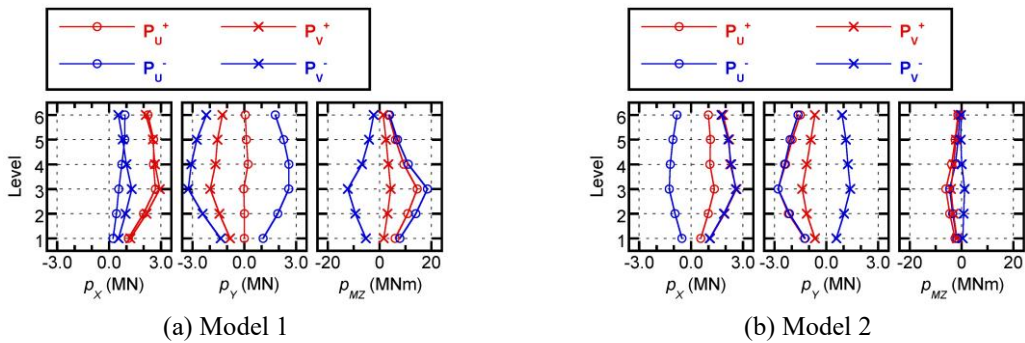


Fig. 10 Combined force distributions used in step 5

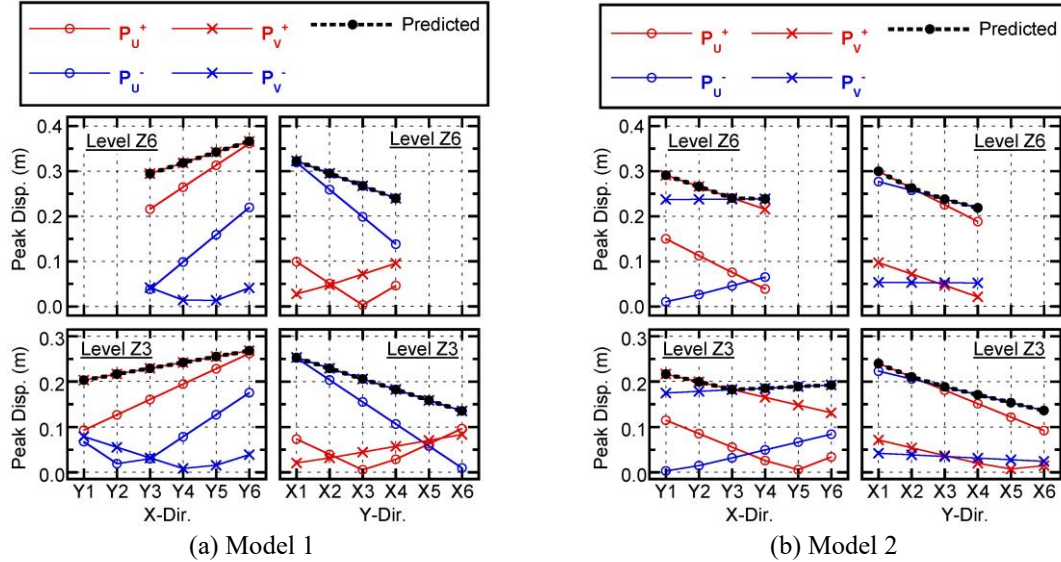


Fig. 11 Distribution of the peak relative horizontal displacements at each frame estimated by the envelope of the four pushover analyses results

4.2 Nonlinear dynamic analysis results

4.2.1 Nonlinear dynamic analysis cases

To evaluate the ability of the simplified procedure to predict the peak displacement response of asymmetric buildings with bidirectional setback, nonlinear dynamic (time-history) analyses were performed in the following steps. First, nonlinear dynamic analyses were carried out for seismic input with various angles of incidence. Then, the envelopes of the peak responses for each angle were obtained from the maximum of the peak responses obtained for three artificial ground motion sets in each angle. Finally, the envelopes of the peak response were compared with the peak responses estimated by the simplified procedure (section 4.1).

Note that the angle of incidence of the “major” component with respect to the X axis, ψ , varies at 15° intervals from (ψ_1-90°) to (ψ_1+90°) , where ψ_1 is the angle of incidence of the U axis corresponding to $D_{1U}^*_{max}$: $\psi_1=-36.6^\circ$ for Model 1 while $\psi_1=89.1^\circ$ for Model 2. Therefore, $3 \times 13 = 39$ cases were considered for the nonlinear dynamic analyses for each building model.

4.2.2 Variation of the peak response with changes in the angle of incidence of the seismic input

Fig. 12 shows the variation of the peak relative horizontal displacement (from basement) of the frames in the X and Y directions with changes in the angle of incidence of the seismic input for Model 1. In this figure, the peak displacement of frames Y6, X1 at level Z6 and X6 at level Z3 are shown.

In Model 1, the largest peak of frame Y6 occurs in the case of $\psi=\psi_1=-36.6^\circ$, which is the principal direction of the first mode corresponding to the predicted peak response. However, the largest peak response of frame X1 occurs when $\psi=-111.6^\circ$, and that of frame X6 occurs when $\psi=-96.6^\circ$.

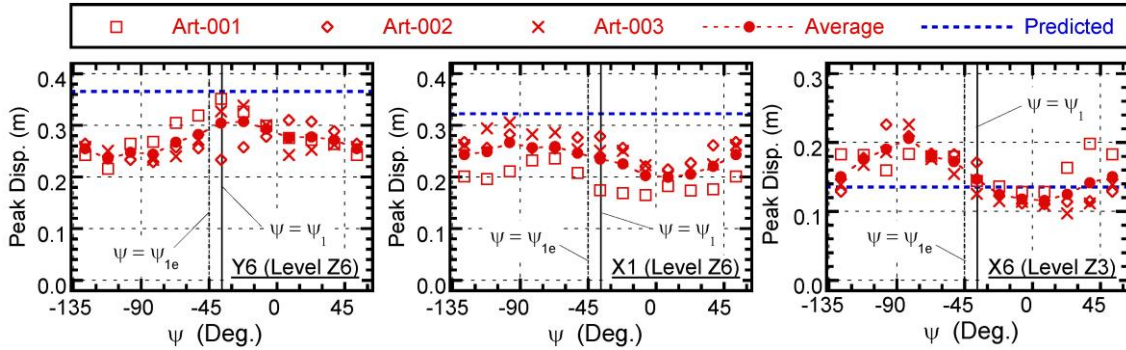


Fig. 12 Variation of the peak relative horizontal displacement of Model 1 with changing angle of incidence of the “major” component for three ground motions Art-001–003. Dashed blue line shows peak displacement estimated by the simplified method

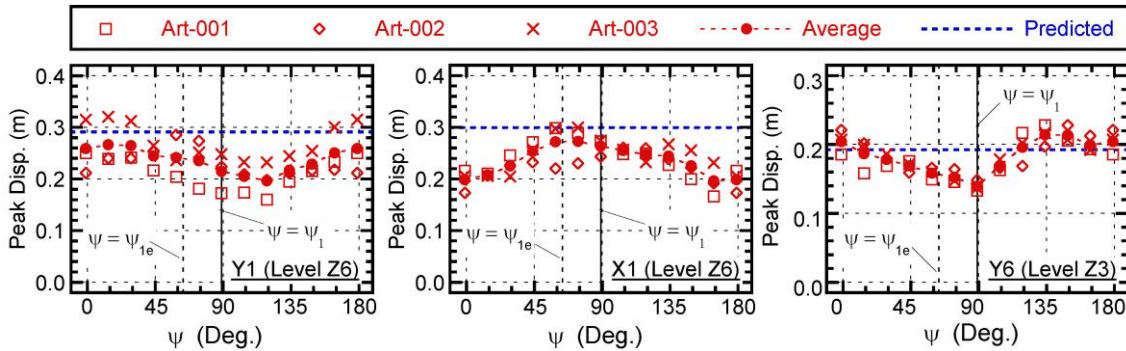


Fig. 13 Variation of the peak relative horizontal displacement of Model 2 with changing angle of incidence of the “major” component for three ground motions Art-001–003. Dashed blue line shows peak displacement estimated by the simplified method

Fig. 13 shows the variation of the peak relative horizontal displacement of the frames in the X and Y directions with changes in the angle of incidence of the seismic input for Model 2. In this figure, the peak displacement of frames Y1, X1 at level Z6 and Y6 at level Z3 are shown.

In Model 2, the largest peak response of frame X1 in level Z6 occurs when $\psi=74.1^\circ$, which is between the principal direction of the first mode in the elastic range $\psi_{1e} (=63.6^\circ)$ and that corresponding to the predicted peak response $\psi_1 (=89.1^\circ)$. However, the largest peak response of frame Y1 occurs when $\psi=14.1^\circ$, and that of frame Y6 occurs when $\psi=164.1^\circ$. Thus, the variation of the peak response with varying angle of incidence of the seismic input depends on each frame.

4.2.3 Comparison of the peak response predicted by the simplified procedure with that of the dynamic analysis results

Fig. 14 compares the peak relative horizontal displacement at each frame estimated by the simplified procedure with that obtained from the envelope of the dynamic analyses results. For Model 1 (Fig. 14(a)), the largest peak response estimated by the simplified method is conservative except for frames X5 and X6 in level Z3. However, for Model 2 (Fig. 14(b)) the largest peak response agrees very well with the envelope of the dynamic analysis results.

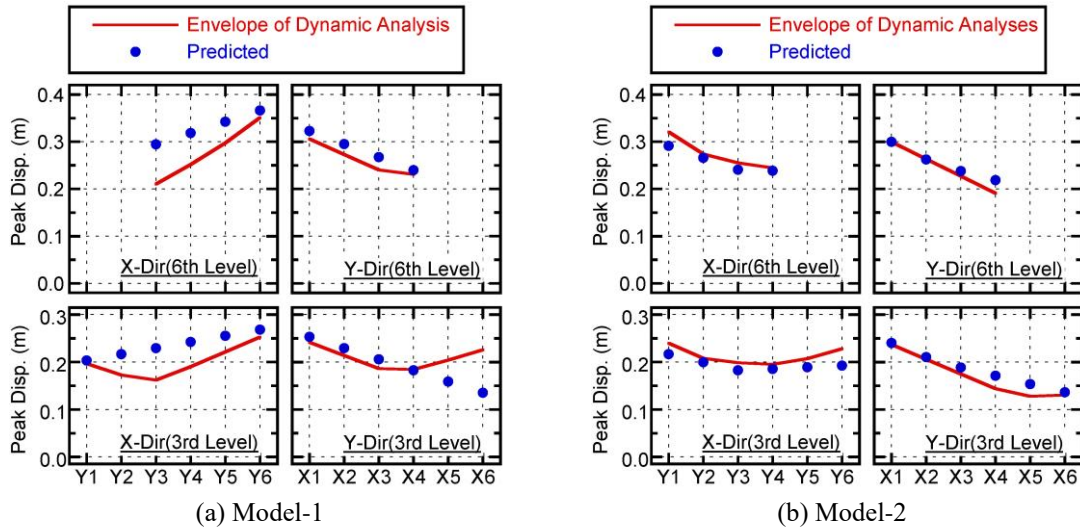


Fig. 14 Comparison of the peak relative horizontal displacement estimated by the simplified procedure at each frame with that derived by the dynamic analysis method

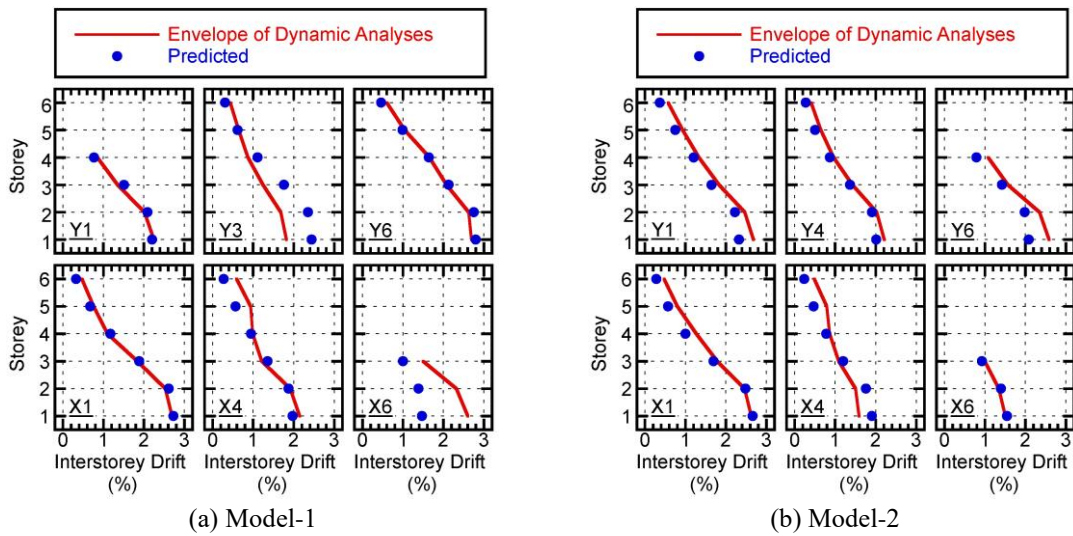


Fig. 15 Comparison of the interstorey drift of frames in the X and Y direction estimated by the simplified procedure at each frame with that derived by the dynamic analysis method

Fig. 15 shows the peak interstorey drift for Model 1 (Fig. 15(a)) and Model 2 (Fig. 15(b)), obtained from the envelope of dynamic analyses results, along with the estimates of the simplified procedure.

In Model 1, the estimated peak response of frames Y6 and X1, where the largest response occurs in the X and Y directions, respectively, agrees well with the envelope of the dynamic analysis results. However, the peak response estimated by the simplified procedure for frame X6 is notably smaller than that derived by the dynamic analysis envelope. In Model 2, the peak

responses of frames Y1 and X1 estimated by the two methods are in good agreement. For frame Y6, the peak response predicted by the simplified procedure is smaller than the envelope of dynamic analysis results; however, the difference between the two methods is small.

These results show that the largest peak response of the two building models investigated in this study is satisfactorily predicted by the simplified procedure, especially the peak response of “flexible-edge” frames. Note that the underestimation of “stiff-edge” frame in one direction (frame X6 in Model 1 and frame Y6 in Model 2) is because the contribution of modes higher than the third mode is neglected in this simplified procedure, as discussed in the previous study (Fujii 2014): in the frame at “stiff-edge”, the contribution of the third mode is significant.

5. Suitability assessment of the simplified procedure based on pushover analysis results

As described in Fujii (2014), there are two critical assumptions in the simplified procedure: (1) the building oscillates predominantly in one mode in each set of orthogonal directions, and (2) the principal directions of the first and second modal responses are almost orthogonal. In this following part, the suitability of the simplified procedure to the two building models are examined from the point of these two assumptions.

From the DB-MAP analysis results in step 1 of the simplified procedure, the second and third modes at loading step n , ${}_n\Phi_2$ and ${}_n\Phi_3$, respectively, were calculated in terms of the displacement vector at step n , ${}_n\mathbf{d}$, and the second and third modes in the elastic range, Φ_{2e} and Φ_{3e} respectively, as Eqs. (9) and (10)

$${}_n\Phi_2 = \Phi_{2e} - \frac{\Phi_{2e}^T \mathbf{M}_n \Phi_1}{{}_n\Phi_1^T \mathbf{M}_n \Phi_1} {}_n\Phi_1 = \Phi_{2e} - \frac{\Phi_{2e}^T \mathbf{M}_n \mathbf{d}}{{}_n\mathbf{d}^T \mathbf{M}_n \mathbf{d}} {}_n\mathbf{d}, \quad (9)$$

$${}_n\Phi_3 = \Phi_{3e} - \frac{\Phi_{3e}^T \mathbf{M}_n \Phi_1}{{}_n\Phi_1^T \mathbf{M}_n \Phi_1} {}_n\Phi_1 - \frac{\Phi_{3e}^T \mathbf{M}_n \Phi_2}{{}_n\Phi_2^T \mathbf{M}_n \Phi_2} {}_n\Phi_2 = \Phi_{3e} - \frac{\Phi_{3e}^T \mathbf{M}_n \mathbf{d}}{{}_n\mathbf{d}^T \mathbf{M}_n \mathbf{d}} {}_n\mathbf{d} - \frac{\Phi_{3e}^T \mathbf{M}_n \Phi_2}{{}_n\Phi_2^T \mathbf{M}_n \Phi_2} {}_n\Phi_2. \quad (10)$$

Next, the i th effective modal mass ratio with respect to the principal direction of the i th modal response at loading step n , the tangent of the angle of incidence of the principal direction of the i th modal response at loading step n , and the torsional index of the i th mode at loading step n , were calculated as Eqs. (11)-(13)

$${}_n m_i^* = \frac{1}{\sum_j m_j} \cdot \frac{\left(\sum_j m_j {}_n\phi_{Xji} \right)^2 + \left(\sum_j m_j {}_n\phi_{Yji} \right)^2}{\sum_j m_j {}_n\phi_{Xji}^2 + \sum_j m_j {}_n\phi_{Yji}^2 + \sum_j I_j {}_n\phi_{\Theta ji}^2}, \quad (11)$$

$$\tan {}_n\psi_i = - \frac{\sum_j m_j {}_n\phi_{Yji}}{\sum_j m_j {}_n\phi_{Xji}}, \quad (12)$$

$${}_n R_{\rho i} = \sqrt{\frac{\sum_j I_j {}_n\phi_{\Theta ji}^2}{\left(\sum_j m_j {}_n\phi_{Xji}^2 + \sum_j m_j {}_n\phi_{Yji}^2 \right)}}. \quad (13)$$

Fig. 16 shows the change of ${}_n m_i^*$, ${}_n\psi_i$, and ${}_n R_{\rho i}$ at each loading step for both models. The dots

“●” in this figure correspond to the points of the peak response of the first mode as estimated by the simplified method, $D_{1U}^*_{max}$.

In Fig. 16(a) ${}_n m_1^*$ varies within the range 0.63-0.70, ${}_n m_2^*$ is almost constant at 0.86 while ${}_n m_3^*$ varies within the range 0.18-0.27, from the elastic range to the point corresponding to the simplified method peak in case of Model 1. The change of ${}_n \psi_i$ is very small, and the angle between the principal directions of the first and second modes is almost 90° . Thus, as discussed in Fujii (2016), Model 1 may oscillate predominantly in the first mode when the unidirectional excitation acts in the principal direction of the first modal response (U axis), while it may oscillate predominantly in the second mode when the unidirectional excitation acts in the orthogonal direction to the principal direction of the first modal response (V axis). The torsional indices ${}_n R_{\rho 1}$ and ${}_n R_{\rho 2}$ vary within the ranges 0.36-0.52 and 0.03-0.09, while ${}_n R_{\rho 3}$ varies within 1.39-1.69. Therefore, the first and second modes of Model 1 are predominantly translational modes (${}_n R_{\rho i} < 1$) while its third mode is predominantly a torsional mode (${}_n R_{\rho 3} > 1$) from the elastic range to the point corresponding to $D_{1U}^*_{max}$. The trend of Model 2 (Fig. 16(b)) is similar to that of Model 1, although ${}_n \psi_1$ varies from 63.6° to 89.1° while ${}_n \psi_2$ varies from -26.4° to -1.0° .

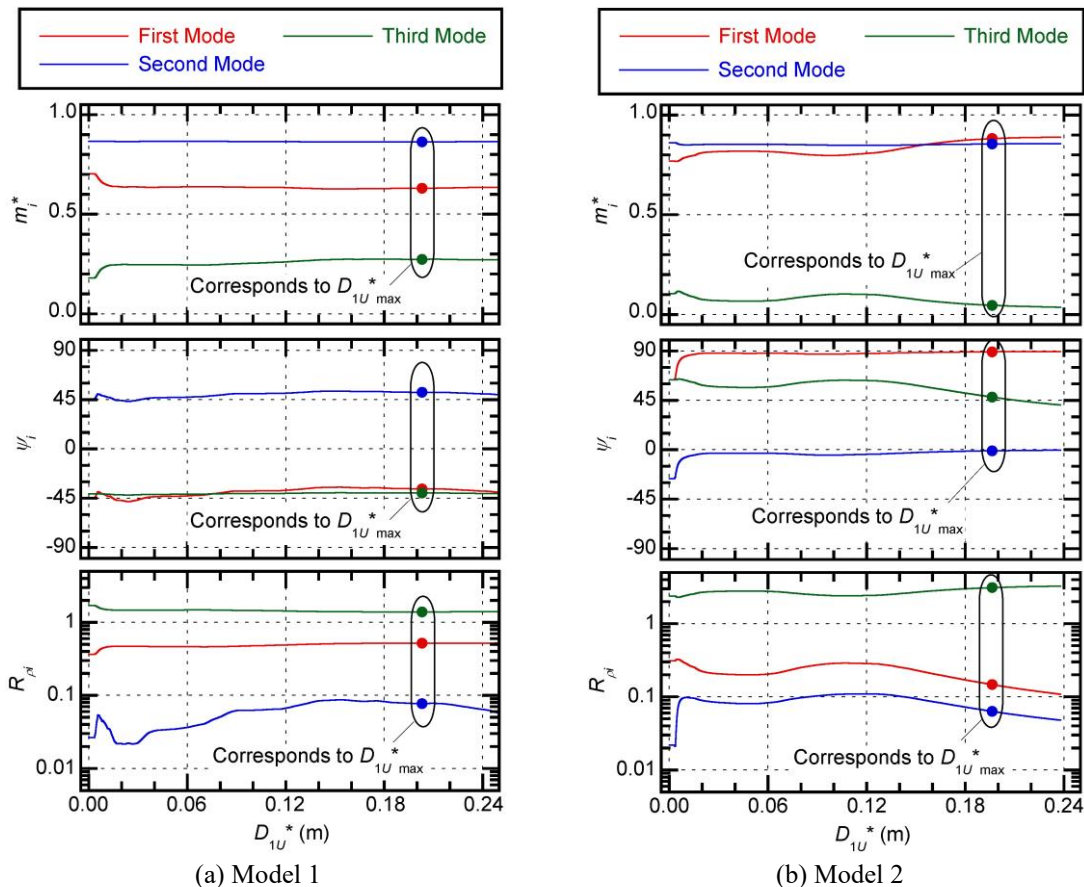


Fig. 16 Change in the effective modal mass ratio, the principal directions of modal responses and the torsional index evaluated from the pushover analysis results. The coloured dots represent the points of the peak response of the first mode as estimated by the simplified method, $D_{1U}^*_{max}$

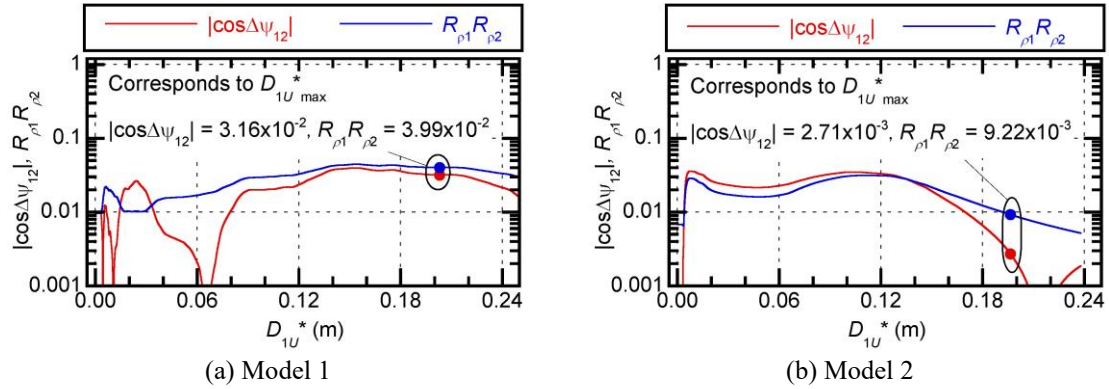


Fig. 17 $|\cos\Delta\psi_{12}|$ and the product $R_{\rho_1}R_{\rho_2}$ evaluated from pushover analyses. The coloured dots represent the values estimated by the simplified method

In the previous study by the author (Fujii 2016), the following interesting relationships were found for a single-story asymmetric building model

$$|\cos\Delta\psi_{12}| = R_{\rho_1}R_{\rho_2}, \quad (14)$$

where $\Delta\psi_{12}$ is the angle between the principal directions of the first and second modes. This implies that if the product of the torsional indices of the first and second modes is close to zero, the principal directions of the first and second modes are almost orthogonal. Strictly speaking, this relation is valid only for the single-story asymmetric building model. However, if the product $R_{\rho_1}R_{\rho_2}$ can approximate $|\cos\Delta\psi_{12}|$ for a multi-storey building model with setback, Eq. (14) can be very useful to evaluate the orthogonality of the principal directions of the first and second modes.

Fig. 17 shows $|\cos\Delta\psi_{12}|$ and $R_{\rho_1}R_{\rho_2}$ evaluated from the pushover analyses results.

The $|\cos\Delta\psi_{12}|$ values are very small from the elastic range to the point corresponding to the simplified method peak: $0 < |\cos\Delta\psi_{12}| < 0.04$ for both Models 1 and 2. This confirms that the principal directions of the first and second modes are close to orthogonal throughout the response. The behaviour of $R_{\rho_1}R_{\rho_2}$ is similar to that of $|\cos\Delta\psi_{12}|$. For Model 1 (Fig. 17(a)), $R_{\rho_1}R_{\rho_2}$ corresponding to the simplified method peak response is 3.99×10^{-2} , while $|\cos\Delta\psi_{12}|$ is 3.16×10^{-2} . Similar trends can be found for Model 2 (Fig. 17(b)); the product $R_{\rho_1}R_{\rho_2}$ corresponding to the simplified method peak response is 9.22×10^{-3} , while $|\cos\Delta\psi_{12}|$ is 2.71×10^{-3} . These results indicate that the product $R_{\rho_1}R_{\rho_2}$ may be used as an index for the evaluation of the orthogonality of the principal directions of the first and second modes.

In conclusion, the two asymmetric building models analysed in this study satisfy the following two conditions; (a) their first and second modes are predominantly translational modes while its third mode is predominantly a torsional mode, and (b) their principal directions of the first and second modal responses are almost orthogonal. It should be note that, Eq. (14) implies that the orthogonality of the principal axes of the first and second modal response is strongly related to the torsional indices R_{ρ_1} and R_{ρ_2} ; if the first or second mode is predominantly torsional mode (R_{ρ_1} or $R_{\rho_2} > 1$), the principal directions of the first and second modes would be far from orthogonal. Besides, it is evident that from Eq. (4), the effective modal mass ratio of the i th mode with respect to the principal direction of the i th modal response, m_i^* will be small when the i th mode is the predominantly torsional mode. Therefore, it is very important to note that these two conditions may not discuss

independently, in case of buildings designed according to weak-beam strong column concept.

6. Conclusions

The suitability of the simplified pushover-based procedure, proposed by the author (Fujii 2014), to asymmetric buildings with bidirectional setback and designed according to weak-beam strong column concept is assessed in this study. In the numerical examples, nonlinear time history analysis of two six-storey asymmetric buildings with bidirectional setback are carried out considering various directions of seismic input. These results are compared with the results estimated by the proposed method. Although the number of building models considered in this study is limited, the following findings are made.

- The largest peak response of the two building models with bidirectional setback investigated in this study is satisfactorily predicted by the simplified pushover-based procedure. Especially, the peak response at the frames where the larger response is expected when building oscillate in the first mode (“flexible-edge” frame) can be predicted with high accuracy by the presented simplified procedure. However, the peak response at the “stiff-edge” frame in one direction may be underestimated by the this procedure.

- The simplified pushover-based procedure is suitable for an asymmetric building with bidirectional setback and designed according to weak-beam strong column concept, if (a) its first and second modes are “predominantly translational” modes while its third mode is a “predominantly torsional” mode, and (b) the principal directions of the first and second modes are almost orthogonal.

- The orthogonality of the principal directions of the first and second modes may be evaluated by the product of the torsional indices of the first and second modes, even for a building with setback.

Note that those two building models considered in this study are designed for seismic resistance according to weak-beam strong column concept. This is because the author have intended to avoid the problems caused by the storey mechanism in this article; the storey mechanism in upper storey may lead the effect of higher modes more significant, so the discussions of the applicability of this simplified pushover-based procedure would be more complicated. Therefore, in this phase, the achievement of this study should be limited within the newer buildings according to weak-beam strong column concept. Applicability to this simplified procedure to the existing buildings, which is not designed according to weak-beam strong column concept, should be studied in the later works. The author is planning the seismic assessment of the exiting irregular building severely damaged in recent earthquakes, e.g., the Uto city office building damaged due to 2016 Kumamoto Earthquake, Japan, as the next phase of this study.

It should be also noted that the results presented in this article are those obtained by using the artificial ground motions whose response spectrum are well fit to the target spectrum. However, the shape of response spectrum of the real ground motions recorded in the past earthquakes, in general, differ significantly from the target spectrum. The author thinks, when the largest peak response considering all possible angle of incidence of the seismic input is needed, the use of the largest response spectrum considering all possible angle for the prediction of the peak response of the first and second mode would provide the conservative results. Or, when the average of peak response considering all possible angle is needed, the use of the geometric mean spectrum of major and minor spectrum for the prediction of the peak response would provide the reasonable

results. However, these expectations should be verified in the later works.

Further studies are needed for the suitability assessment of more complex structural systems such as a frame-wall system with setbacks or with various dampers. The estimation of member forces (shear forces of RC members or bending moments of member ends with no potential hinge) should also be studied in the next phase.

References

- AIJ (1999), Design Guidelines for Earthquake Resistant Reinforced Concrete Buildings Based on Inelastic Displacement Concept, Architectural Institute of Japan, Tokyo, Japan. (in Japanese)
- Anagnostopoulos, S.A., Kyrkos, M.T. and Stathopoulos, K.G. (2015), "Earthquake induced torsion in buildings: critical review and state of the art", *Earthq. Struct.*, **8**(2), 305-377.
- Antoniou, S. and Pinho, R. (2004), "Development and verification of a displacement-based adaptive pushover procedure", *J. Earthq. Eng.*, **8**(5), 643-661.
- ATC-40 (1996), Seismic evaluation and retrofit of concrete buildings, Vol. 1, Applied Technology Council, Redwood City, California, USA.
- ASCE (2007), Seismic rehabilitation of existing buildings, American Society of Civil Engineering, Reston, Virginia, USA.
- BCJ (2010), "The Building Standard Law of Japan on CD-ROM", the Building Center of Japan, Tokyo.
- Belejo, A. and Bento, R. (2016), "Improved Modal Pushover Analysis in seismic assessment of asymmetric plan buildings under the influence of one and two horizontal components of ground motions", *Soil Dyn. Earthq. Eng.*, **87**, 1-15.
- Bhatt, C. and Bento, R. (2011), "Assessing the seismic response of existing RC buildings using the extended N2 method", *Bull. Earthq. Eng.*, **9**(4), 1183-1201.
- Bhatt, C. and Bento, R. (2012), "Comparison of nonlinear static methods for the seismic assessment of plan irregular frame buildings with non seismic details", *J. Earthq. Eng.*, **16**(1), 15-39.
- Bhatt, C. and Bento, R. (2014), "The extended adaptive capacity spectrum method for the seismic assessment of plan-asymmetric buildings", *Earthq. Spectra*, **30**(2), 683-703.
- Bosco, M., Ghersi, A. and Marino, E.M. (2012), "Corrective eccentricities for assessment by nonlinear static method of 3D structures subjected to bidirectional ground motion", *Earthq. Eng. Struct. Dyn.*, **41**(13), 1751-1773.
- Bosco, M., Marino, E.M. and Ghersi, A. (2013), "An analytical method for evaluation of the in-plan irregularity of non-regularly asymmetric buildings", *Bull. Earthq. Eng.*, **11**(5), 1423-1445.
- Bosco, M., Marino, E.M. and Ghersi, A. (2015), "Predicting displacement demand of multi-storey asymmetric buildings by nonlinear static analysis and corrective eccentricities", *Eng. Struct.*, **99**, 373-387.
- CEN (2004) Eurocode 8 - design of structures for earthquake resistance, Part 1: general rules, seismic actions and rules for buildings, European standard EN 1998-1, European Committee for Standardization, Brussels, Belgium.
- Chopra, A.K. and Goel, R.K. (2002), "A modal pushover analysis procedure for estimating seismic demands for buildings", *Earthq. Eng. Struct. Dyn.*, **31**(3), 561-582.
- Chopra, A.K. and Goel, R.K. (2004), "A modal pushover analysis procedure to estimate seismic demands for unsymmetric-plan buildings", *Earthq. Eng. Struct. Dyn.*, **33**(8), 903-927.
- Cimellaro, G.P., Giovine, T. and Lopez-Garcia, D. (2014), "Bidirectional pushover analysis of irregular structures", *J. Struct. Eng.*, ASCE, **140**(9), doi: 10.1061/(ASCE)ST.1943-541X.0001032.
- D'Ambrisi, A., De Stefano, M. and Tanganelli, M. (2009), "Use of pushover analysis of predicting seismic response of irregular buildings: a case study", *J. Earthq. Eng.*, **13**(8), 1089-1100.
- De Stefano, M. and Pintucchi, B. (2008), "A review on seismic behaviour of irregular building structure since 2002", *Bull. Earthq. Eng.*, **6**(2), 285-308.
- De Stefano, M. and Pintucchi, B. (2010), "Predicting torsion-induced lateral displacements for pushover

- analysis: Influence of torsion system characteristics”, *Earthq. Eng. Struct. Dyn.*, **39**(12), 1369-1394.
- Fajfar, P. and Fischinger, M. (1988), “N2-a method for non-linear seismic analysis of regular buildings”, *Proceedings of ninth world conference on earthquake engineering*, Tokyo-Kyoto, Japan, August.
- Fajfar, P., Marušić, D. and Peruš, I. (2005), “Torsional effects in the pushover-based seismic analysis of buildings”, *J. Earthq. Eng.*, **9**(6), 831-854.
- FEMA (1997), NEHRP guidelines for the seismic rehabilitation of buildings, FEMA Publication 273, Federal Emergency Management Agency, Washington, D.C., USA.
- Fujii, K. (2011), “Nonlinear static procedure for multi-story asymmetric frame buildings considering bidirectional excitation”, *J. Earthq. Eng.*, **15**(2), 245-273.
- Fujii, K. (2014), “Prediction of the largest peak nonlinear seismic response of asymmetric buildings under bi-directional excitation using pushover analyses”, *Bull. Earthq. Eng.*, **12**(2), 909-938.
- Fujii, K. (2015), “Application of the pushover-based procedure to predict the largest peak response of asymmetric buildings with buckling-restrained braces”, *5th International Conference on Computational Methods in Structural Dynamics and Earthquake Engineering (COMPDYN 2015)*, Crete Island, Greece, May.
- Fujii, K. (2016), “Torsional index of an asymmetric building based on mode shape”, *Seismic Behaviour and Design of Irregular and Complex Civil Structures II*, Springer, 99-109.
- Isakovic, T. and Fischinger, M. (2011), “Applicability of pushover methods to the seismic analysis of an RC bridge, experimentally tested on three shake tables”, *J. Earthq. Eng.*, **15**(2), 303-320.
- Kreslin, M. and Fajfar, P. (2010), “Seismic evaluation of an existing complex RC building”, *Bull. Earthq. Eng.*, **8**(2), 363-385.
- Kreslin, M. and Fajfar, P. (2012), “The extended N2 method considering higher mode effects in both plan and elevation”, *Bull. Earthq. Eng.*, **10**(2), 695-715.
- Lavan, O. and De Stefano, M. (Eds.) (2013), *Seismic Behaviour and Design of Irregular and Complex Civil Structures*, Springer, Dordrecht, Nederland.
- López, A., Hernández, J.J., Bonilla, R. and Fernández, A. (2006), “Response spectra for multicomponent structural analysis”, *Earthq. Spectra*, **22**(1), 85-113.
- Manoukas, G., Athanatopoulou, A. and Avramidis, I. (2012), “Multimode pushover analysis for asymmetric buildings under biaxial seismic excitation based on a new concept of the equivalent single degree of freedom system”, *Soil Dyn. Earthq. Eng.*, **38**, 88-96.
- Manoukas, G. and Avramidis, I. (2014), “Evaluation of a multimode pushover procedure for asymmetric in plan buildings under biaxial seismic excitation”, *Bull. Earthq. Eng.*, **12**(6), 2607-2632.
- Moghadam, A.S. and Tso, W.K. (1996), “Damage assessment of eccentric multistorey buildings using 3-D pushover analysis”, *Proceedings of 11th world conference on earthquake engineering*, Acapulco, Mexico, June.
- Moghadam, A.S. and Tso, W.K. (2000), “Pushover analysis for asymmetric and set-back multi-story buildings”, *Proceedings of 12th world conference on earthquake engineering*, Auckland, New Zealand, February.
- Muto, K., Hisada, T., Tsugawa, T. and Bessho, S. (1974), “Earthquake resistant design of a 20 story reinforced concrete buildings”, *Proceedings of the 5th world conference on earthquake engineering*, 1960-1969, Rome, Italy, June.
- Penzien, J. and Watabe, M. (1975), “Characteristics of 3-dimensional earthquake ground motions”, *Earthq. Eng. Struct. Dyn.*, **3**(4), 365-373.
- Peruš, I. and Fajfar, P. (2005), “On the inelastic torsional response of single-storey structures under bi-axial excitation”, *Earthq. Eng. Struct. Dyn.*, **34**(8), 931-941.
- Reyes, J.C. and Chopra, A.K. (2011a), “Three-dimensional modal pushover analysis of buildings subjected to two components of ground motion, including its evaluation for tall buildings”, *Earthq. Eng. Struct. Dyn.*, **40**(7), 789-806.
- Reyes, J.C. and Chopra, A.K. (2011b), “Evaluation of three-dimensional modal pushover analysis for unsymmetric-plan buildings subjected to two components of ground motion”, *Earthq. Eng. Struct. Dyn.*, **40**(13), 1475-1494.

- Saiidi, M. and Sozen, M.A. (1981), "Simple nonlinear seismic analysis of R/C structures", *J. Struct. Div.*, ASCE, **107**(5), 937-952.
- Zembaty, Z. and De Stefano, M. (Eds.) (2015), *Seismic Behaviour and Design of Irregular and Complex Civil Structures II*, Springer, Dordrecht, Nederland.

SA

Appendix: Longitudinal reinforcement of each member

Tables 1-3 show the list of longitudinal reinforcement of each member for Models 1 and 2. Note that the contribution of slab reinforcement (2-D10+2-D13 for the perimeter beams, while 4-D10+4-D13 for the inner beams) is considered for the calculation of yield moment M_y (tension in upper side) of the beams in level Z1 to Z6.

Table 1 Longitudinal reinforcement of beams (Model 1)

Level	Longitudinal reinforcement (top and bottom sides)												
	Frame (X-dir.)						Frame (Y-Dir.)						
	Y1	Y2	Y3	Y4	Y5	Y6	X1	X2	X3	X4	X5	X6	
Z6			3-D25	3-D25	3-D25	3-D25	3-D25	3-D25	3-D25	3-D25	3-D25		
Z5		3-D25	4-D25	4-D25	4-D25	4-D25	3-D25	3-D25	3-D25	3-D25			
Z4	3-D25	5-D25	5-D25	5-D25	5-D25	5-D25	4-D25	4-D25	4-D25	4-D25			
Z3	4-D25	5-D25	5-D25	5-D25	5-D25	5-D25	5-D25	5-D25	5-D25	5-D25	5-D25	4-D25	4-D25
Z2	5-D25	5-D25	5-D25	5-D25	5-D25	5-D25	5-D25	5-D25	5-D25	5-D25	5-D25	5-D25	5-D25
Z1	5-D25	5-D25	5-D25	5-D25	5-D25	5-D25	5-D25	5-D25	5-D25	5-D25	5-D25	5-D25	5-D25
Z0	6-D25	6-D25	6-D25	6-D25	6-D25	6-D25	6-D25	6-D25	6-D25	6-D25	6-D25	6-D25	6-D25

Table 2 Longitudinal reinforcement of beams (Model 2)

Level	Longitudinal reinforcement (top and bottom sides)												
	Frame (X-dir.)						Frame (Y-Dir.)						
	Y1	Y2	Y3	Y4	Y5	Y6	X1	X2	X3	X4	X5	X6	
Z6	3-D25	3-D25	3-D25	3-D25			3-D25	3-D25	3-D25	3-D25			
Z5	4-D25	4-D25	4-D25	4-D25	3-D25		3-D25	3-D25	3-D25	3-D25			
Z4	3-D25	5-D25	5-D25	5-D25	5-D25	3-D25	4-D25	4-D25	4-D25	4-D25			
Z3	4-D25	5-D25	5-D25	5-D25	5-D25	4-D25	5-D25	5-D25	5-D25	5-D25	5-D25	4-D25	4-D25
Z2	5-D25	5-D25	5-D25	5-D25	5-D25	5-D25	5-D25	5-D25	5-D25	5-D25	5-D25	5-D25	5-D25
Z1	5-D25	5-D25	5-D25	5-D25	5-D25	5-D25	5-D25	5-D25	5-D25	5-D25	5-D25	5-D25	5-D25
Z0	6-D25	6-D25	6-D25	6-D25	6-D25	6-D25	6-D25	6-D25	6-D25	6-D25	6-D25	6-D25	6-D25

Table 3 Longitudinal reinforcement of columns (Models 1 and 2)

Storey	Longitudinal reinforcement
2nd to 6th	20-D29 (top and bottom)
1	20-D29 (top), 12-D29 (bottom)